Biomedical Optics EXPRESS

Biocompatible near-infrared fluorescent nanoparticles for macro and microscopic *in vivo* functional bioimaging

Liliang Chu,[1] Shaowei Wang,[1] Kanghui Li,[1] Wang Xi,[2] Xinyuan Zhao,[3] and Jun Qian[1,*]

[1] *State Key Laboratory of Modern Optical Instrumentations, Centre for Optical and Electromagnetic Research, Zhejiang University; Zhejiang Provincial Key Laboratory for Sensing Technologies; Joint Research Center of Photonics of the Royal Institute of Technology (Sweden) and Zhejiang University, Zijingang Campus, Zhejiang University, Hangzhou 310058, China*

[2]*Department of Neurobiology, School of Medicine, Zhejiang University, Zijingang Campus, Hangzhou 310058, China*

[3]*Bioelectromagnetics Laboratory, School of Medicine, Zhejiang University, Hangzhou 310058, China*

[*]*qianjun@zju.edu.cn*

Abstract: Near-infrared (NIR) imaging technology has been widely used for biomedical research and applications, since it can achieve deep penetration in biological tissues due to less absorption and scattering of NIR light. In our research, polymer nanoparticles with NIR fluorophores doped were synthesized. The morphology, absorption/emission features and chemical stability of the fluorescent nanoparticles were characterized, separately. NIR fluorescent nanoparticles were then utilized as bright optical probes for macro *in vivo* imaging of mice, including sentinel lymph node (SLN) mapping, as well as distribution and excretion monitoring of nanoparticles in animal body. Furthermore, we applied the NIR fluorescent nanoparticles in *in vivo* microscopic bioimaging via a confocal microscope. Under the 635 nm-CW excitation, the blood vessel architecture in the ear and the brain of mice, which were administered with nanoparticles, was visualized very clearly. The imaging depth of our one-photon microscopy, which was assisted with NIR fluorescent nanoprobes, can reach as deep as 500 μm. Our experiments show that NIR fluorescent nanoparticles have great potentials in various deep-tissue imaging applications.

OCIS codes: (160.2540) Fluorescent and luminescent materials; (160.4236) Nanomaterials; (300.6170) Spectra; (170.3880) Medical and biological imaging; (170.2655) Functional monitoring and imaging; (180.1790) Confocal microscopy.

References and links

1. J. R. Lakowicz, *Principles of Fluorescence Spectroscopy* (Springer, New York, 2006).
2. S. W. Hell, "Far-field optical nanoscopy," Science **316**(5828), 1153–1158 (2007).
3. M. G. L. Gustafsson, "Nonlinear structured-illumination microscopy: Wide-field fluorescence imaging with theoretically unlimited resolution," Proc. Natl. Acad. Sci. U.S.A. **102**(37), 13081–13086 (2005).
4. M. J. Rust, M. Bates, and X. W. Zhuang, "Sub-diffraction-limit imaging by stochastic optical reconstruction microscopy (STORM)," Nat. Methods **3**(10), 793–796 (2006).
5. E. Betzig, G. H. Patterson, R. Sougrat, O. W. Lindwasser, S. Olenych, J. S. Bonifacino, M. W. Davidson, J. Lippincott-Schwartz, and H. F. Hess, "Imaging intracellular fluorescent proteins at nanometer resolution," Science **313**(5793), 1642–1645 (2006).
6. D. Axelrod, "Total internal reflection fluorescence microscopy in cell biology," Traffic **2**(11), 764–774 (2001).
7. R. Splinter and B. A. Hooper, *An Introduction to Biomedical Optics* (CRC Press, 2006).
8. A. Yodh and B. Chance, "Spectroscopy and imaging with diffusing light," Phys. Today **48**(3), 34–40 (1995).
9. R. Weissleder, "A clearer vision for in vivo imaging," Nat. Biotechnol. **19**(4), 316–317 (2001).
10. E. M. Sevick-Muraca, J. P. Houston, and M. Gurfinkel, "Fluorescence-enhanced, near infrared diagnostic imaging with contrast agents," Curr. Opin. Chem. Biol. **6**(5), 642–650 (2002).
11. W. B. Cai, D. W. Shin, K. Chen, O. Gheysens, Q. Z. Cao, S. X. Wang, S. S. Gambhir, and X. Y. Chen, "Peptide-labeled near-infrared quantum dots for imaging tumor vasculature in living subjects," Nano Lett. **6**(4), 669–676 (2006).

#222817 - $15.00 USD Received 10 Sep 2014; revised 22 Oct 2014; accepted 23 Oct 2014; published 28 Oct 2014

12. K. T. Yong, I. Roy, H. Ding, E. J. Bergey, and P. N. Prasad, "Biocompatible Near-Infrared Quantum Dots as Ultrasensitive Probes for Long-Term in vivo Imaging Applications," Small **5**(17), 1997–2004 (2009).
13. M. Nyk, R. Kumar, T. Y. Ohulchanskyy, E. J. Bergey, and P. N. Prasad, "High Contrast in Vitro and in Vivo Photoluminescence Bioimaging Using Near Infrared to Near Infrared Up-Conversion in Tm^{3+} and Yb^{3+} Doped Fluoride Nanophosphors," Nano Lett. **8**(11), 3834–3838 (2008).
14. B. Dubertret, P. Skourides, D. J. Norris, V. Noireaux, A. H. Brivanlou, and A. Libchaber, "In vivo imaging of quantum dots encapsulated in phospholipid micelles," Science **298**(5599), 1759–1762 (2002).
15. M. Dahan, S. Lévi, C. Luccardini, P. Rostaing, B. Riveau, and A. Triller, "Diffusion dynamics of glycine receptors revealed by single-quantum dot tracking," Science **302**(5644), 442–445 (2003).
16. J. Lovrić, S. J. Cho, F. M. Winnik, and D. Maysinger, "Unmodified Cadmium Telluride Quantum Dots Induce Reactive Oxygen Species Formation Leading to Multiple Organelle Damage and Cell Death," Chem. Biol. **12**(11), 1227–1234 (2005).
17. R. Hardman, "A toxicologic review of quantum dots: Toxicity depends on physicochemical and environmental factors," Environ. Health Perspect. **114**(2), 165–172 (2006).
18. Y. P. Du, B. Xu, T. Fu, M. Cai, F. Li, Y. Zhang, and Q. B. Wang, "Near-Infrared Photoluminescent Ag_2S Quantum Dots from a Single Source Precursor," J. Am. Chem. Soc. **132**(5), 1470–1471 (2010).
19. X. Zhang, Y. Q. Gu, and H. Y. Chen, "Synthesis of biocompatible near infrared fluorescence Ag_2S quantum dot and its application in bioimaging," J. Innov. Opt. Health Sci. **7**(03), 1350059 (2014).
20. M. F. Foda, L. Huang, F. Shao, and H. Y. Han, "Biocompatible and highly luminescent near-infrared $CuInS_2$/ZnS quantum dots embedded silica beads for cancer cell imaging," ACS Appl. Mater. Interfaces **6**(3), 2011–2017 (2014).
21. W. Feng, X. J. Zhu, and F. Y. Li, "Recent advances in the optimization and functionalization of upconversion nanomaterials for in vivo bioapplications," NPG Asia Mater. **5**(12), e75 (2013).
22. J. Zhou, Z. Liu, and F. Y. Li, "Upconversion nanophosphors for small-animal imaging," Chem. Soc. Rev. **41**(3), 1323–1349 (2012).
23. C. T. Xu, P. Svenmarker, H. C. Liu, X. Wu, M. E. Messing, L. R. Wallenberg, and S. Andersson-Engels, "High-Resolution Fluorescence Diffuse Optical Tomography Developed with Nonlinear Upconverting Nanoparticles," ACS Nano **6**(6), 4788–4795 (2012).
24. F. Wang and X. G. Liu, "Recent advances in the chemistry of lanthanide-doped upconversion nanocrystals," Chem. Soc. Rev. **38**(4), 976–989 (2009).
25. A. Poellinger, "Near-infrared imaging of breast cancer using optical contrast agents," J. Biophotonics **5**(11-12), 815–826 (2012).
26. J. O. Escobedo, O. Rusin, S. Lim, and R. M. Strongin, "NIR Dyes for Bioimaging Applications," Curr. Opin. Chem. Biol. **14**(1), 64–70 (2010).
27. R. Kumar, I. Roy, T. Y. Ohulchanskky, L. A. Vathy, E. J. Bergey, M. Sajjad, and P. N. Prasad, "In Vivo Biodistribution and Clearance Studies Using Multimodal Organically Modified Silica Nanoparticles," ACS Nano **4**(2), 699–708 (2010).
28. F. Erogbogbo, K. T. Yong, I. Roy, G. X. Xu, P. N. Prasad, and M. T. Swihart, "Biocompatible luminescent silicon quantum dots for imaging of cancer cells," ACS Nano **2**(5), 873–878 (2008).
29. K. T. Yong, R. Hu, I. Roy, H. Ding, L. A. Vathy, E. J. Bergey, M. Mizuma, A. Maitra, and P. N. Prasa, "Tumor Targeting and Imaging in Live Animals with Functionalized Semiconductor Quantum Rods," ACS. Appl. Mater. Inter. **1**(3), 710–719 (2009).
30. Y. Lei, H. Tang, L. Yao, R. Yu, M. Feng, and B. Zou, "Applications of mesenchymal stem cells labeled with Tat peptide conjugated quantum dots to cell tracking in mouse body," Bioconjug. Chem. **19**(2), 421–427 (2008).
31. R. Kumar, T. Y. Ohulchanskyy, I. Roy, S. K. Gupta, C. Borek, M. E. Thompson, and P. N. Prasad, "Near-Infrared Phosphorescent Polymeric Nanomicelles: Efficient Optical Probes for Tumor Imaging and Detection," ACS Appl. Mater. Interfaces **1**(7), 1474–1481 (2009).
32. J. Qian, D. Wang, F. H. Cai, Q. Q. Zhan, Y. L. Wang, and S. L. He, "Photosensitizer encapsulated organically modified silica nanoparticles for direct two-photon photodynamic therapy and In Vivo functional imaging," Biomaterials **33**(19), 4851–4860 (2012).
33. N. G. Horton, K. Wang, D. Kobat, C. G. Clark, F. W. Wise, C. B. Schaffer, and C. Xu, "In vivo three-photon microscopy of subcortical structures within an intact mouse brain," Nat. Photonics **7**(3), 205–209 (2013).
34. D. Wang, J. Qian, S. L. He, J. S. Park, K. S. Lee, S. H. Han, and Y. Mu, "Aggregation-enhanced fluorescence in PEGylated phospholipid nanomicelles for in vivo imaging," Biomaterials **32**(25), 5880–5888 (2011).
35. J. B. Birks, *Photophysics of Aromatic Molecules* (Wiley, London, 1970).
36. R. Philip, A. Penzkofer, W. Bäumler, R. M. Szeimies, and C. Abels, "Absorption and fluorescence spectroscopic investigation of indocyanine green," J. Photochem. Photobiol. Chem. **96**(1–3), 137–148 (1996).
37. S. Kim, Y. T. Lim, E. G. Soltesz, A. M. De Grand, J. Lee, A. Nakayama, J. A. Parker, T. Mihaljevic, R. G. Laurence, D. M. Dor, L. H. Cohn, M. G. Bawendi, and J. V. Frangioni, "Near-infrared fluorescent type II quantum dots for sentinel lymph node mapping," Nat. Biotechnol. **22**(1), 93–97 (2004).
38. J. Qian, L. Jiang, F. H. Cai, D. Wang, and S. L. He, "Fluorescence-surface enhanced Raman scattering co-functionalized gold nanorods as near-infrared probes for purely optical in vivo imaging," Biomaterials **32**(6), 1601–1610 (2011).
39. K. H. Song, C. Kim, K. Maslov, and L. V. Wang, "Noninvasive in vivo spectroscopic nanorod-contrast photoacoustic mapping of sentinel lymph nodes," Eur. J. Radiol. **70**(2), 227–231 (2009).

#222817 - $15.00 USD Received 10 Sep 2014; revised 22 Oct 2014; accepted 23 Oct 2014; published 28 Oct 2014

1. Introduction

Fluorescence imaging technique occupies an important and unique position in life sciences and medicine [1], due to its advantages for noninvasive study of biological tissues. In addition, fluorescence imaging can provide high spatial resolution [2–5] and high sensitivity [6] of samples. However, the realization of higher resolution is at the expense of short penetration depth in biological tissues [7]. Absorption of biological tissue and water, as well as scattering, limits the focusing capability, and penetration depth of light. To overcome this problem, lots of studies have mainly focused on developing fluorophores in the "optical transmission window" of biological tissue (700 - 900 nm) during past years [8]. Compared with visible light, NIR light is less absorbed/scattered by biological tissue and water, and then has deeper tissue focusing and penetration capability. Furthermore, autofluorescence can be also effectively restrained when NIR light is adopted as an excitation source. Thus, NIR imaging technology is a promising tool for deep-tissue *in vivo* biomedical study [9,10].

Recently, various NIR luminescent nanoparticles have already been applied in biological imaging, such as quantum dots (QDs) [11,12], up-conversion nanoparticles (UCNPs) [13]. QDs possess many advantages: high brightness, good photostability, tunable absorption and emission spectra and a broad spectral excitation range [14,15]. Some NIR QDs composed of heavy metals (e.g. PbSe, PbS and CdTe) have certain cytotoxicity [16,17], which makes them not so suitable for biological imaging. However, some research has been done to synthesize new types of QDs, which are more biocompatible and less harmful to biological cells and tissues, facilitating their applications in deep-tissue bioimaging [18–20]. UCNPs are also widely used in biological imaging [21,22]. Although the luminescent quantum yield of most UCNPs is very low [23], they still provide many advantages for bioimaging applications, such as high signal to noise ratio, superior photostability, tunable luminescence spectrum, as well as sharp absorption and emission lines [24]. Due to facile synthesis process, relatively high fluorescence quantum yield, and convenient chemical modification, organic NIR fluorophores are still the most promising candidates in biomedical imaging area [25]. Unfortunately, most NIR fluorophores cannot be directly used for biological applications, since they are hydrophobic. Many efforts are being made to solve this problem. One way is introducing some hydrophilic groups to the hydrophobic fluorophores to make them aqueously soluble [26]. However, aggregation of fluorophores still occurs when they are injected into animal body. Another promising alternative approach is using aqueously dispersable nanoparticles to encapsulate hydrophobic fluorophores [27], which can overcome the aggregation of fluorophores very effectively. Among various nanoparticles, polymer nanoparticles made up of biocompatible hydrophobic-hydrophilic copolymers (e.g. phospholipids-PEG), are very promising and more suitable for *in vivo* applications [28]. They can be facilely synthesized and conjugated with biomolecules to target certain parts of live animal body (e.g. tumors) [29,30]. They have little cytotoxicity and good biocompatibility [31]. The long PEG chains in polymer nanoparticles can improve the long-time circulation of nanoparticles in an animal body and help to avoid capture/degradation by reticuloendothelial systems (RES).

For deep-tissue *in vivo* microscopy, multi-photon fluorescence microscopy is a very good solution. Relying on the absorption of two or more NIR photons by fluorophores at once, multiphoton microscopy is capable of achieving better focusing, deeper tissue penetration and efficient light detection noninvasively. It has been widely used in thick-tissue and *in vivo* bioimaging [32,33]. However, multi-photon fluorescence is a typical nonlinear optical effect, and high peak power excitation is essential for multi-photon microscopy, which may cause overheating and damage towards biological tissues. In addition, most high peak power pulsed laser sources (e.g. femtosecond laser) are very expensive and sensitive to the working environment, and cannot be easily afforded. In some cases, one-photon confocal microscopy with red light excitation and NIR emission can be another good way to achieve deep-tissue bioimaging. Red excitation light (e.g. 635 nm) is near the "optical transmission window" of

#222817 - $15.00 USD Received 10 Sep 2014; revised 22 Oct 2014; accepted 23 Oct 2014; published 28 Oct 2014

biological tissue (700 - 900 nm). Optical absorption and scattering of red light in biological tissue is not distinct, and its penetration in tissues can be also deep. Furthermore, laser sources for one-photon fluorescence excitation (e.g. 635 nm CW laser) are very safe to bio-samples. They are cost effective, stable in various experimental environments, and easily afforded. In addition, the quantum yield of IR fluorophore under one-photon excitation is usually larger than 0.01 [31], but the quantum yield of some very efficient visible dyes under two-photon excitation is usually less than 10^{-8} [23]. It illustrates IR fluorophore under one-photon excitation has higher fluorescence efficiency, which is helpful to obtain strong imaging signals.

In this paper, IR-820, which is a typical type of NIR fluorophore, was encapsulated in polymer nanoparticles. The morphology of IR-820 doped polymer nanoparticles was characterized. The absorption and fluorescence spectra of the nanoparticles were measured, and their chemical stability was also verified. For macro *in vivo* bioimaging, IR-820 doped polymer nanoparticles were intradermally injected into the forepaw of nude mice for SLN mapping. In addition, they were intravenously injected into live mice via their tail vein, and the whole-body NIR imaging results illustrated that polymer nanoparticles could be excreted from mice body through their hepatobiliary transport. For microscopic *in vivo* bioimaging, mice were also intravenously administered with NIR fluorescent nanoparticles, and all the experiments were performed on a confocal microscope with 635 nm-CW excitation. The blood vessels at various vertical depths in the ear of a BABL/c mouse were observed with high signal to noise ratio. Furthermore, we performed microscopic *in vivo* imaging of the brain of mice. Three-dimensional (3D) reconstructive images of blood architecture were achieved, and the imaging depth of our one-photon confocal microscopy, which was assisted with NIR fluorescent nanoprobes, could reach as deep as 500 μm. The *in vivo* bioimaging results demonstrated that NIR fluorophores doped polymer nanoparticles can be utilized as a good candidate for high-contrast and deep-tissue functional bioimaging.

2. Experimental section

2.1 Synthesis of IR-820 doped polymer nanoparticles

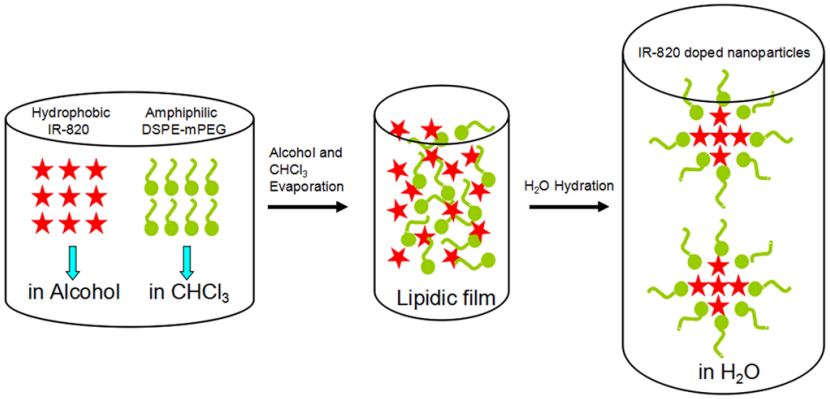

Fig. 1. The scheme illustrating the synthesis procedures of IR-820 doped polymer nanoparticles.

Figure 1 shows the synthesis procedures of IR-820 doped polymer nanoparticles. Typically, 800 μl of IR-820 in ethanol (1 mM) was mixed with 3.2 ml of DSPE-mPEG$_{5000}$ in chloroform (10 mg/mL). The mixture was sonicated for two minutes to form a homogeneous solution, and dried at 70 °C in a rotary evaporator. Next, 500 μl of phosphate buffered saline (PBS, 1X, pH = 7.4) was added into the obtained lipidic film, and the solution was sonicated for five minutes. After that, an optically clear suspension containing IR-820 doped polymer nanoparticles was obtained, which can be used for further experiments.

#222817 - $15.00 USD Received 10 Sep 2014; revised 22 Oct 2014; accepted 23 Oct 2014; published 28 Oct 2014

2.2 Characterization

The structure of IR-820 doped polymer nanoparticles was taken by a JEOL JEM-1230 transmission electron microscopy (TEM) operated at 80 kV in bright field mode. The absorption spectra of nanoparticles were characterized by a Shimadzu 2550 UV-vis scanning spectrophotometer (400 - 900 nm). NIR fluorescence spectra of nanoparticles were characterized by a Maestro *in vivo* optical imaging system (CRI, Inc. Woburn, MA), which consists of an optical head, an optical coupler, a cooled scientific-grade monochrome CCD camera and an image acquisition/analysis software.

2.3 Cell viability analysis

The cytotoxicity of IR-820 doped polymer nanoparticles to HeLa cells was evaluated by following the instructions of cell counting kit-8 (CCK-8). 5000 cells/well in a 100 μl suspension were incubated in 96-well plates for 24 h. Then, a 100 μl fresh culture medium containing nanoparticles with various concentrations ranging from 0 to 4 μg/ml was added into each well. After incubation for 24 h, the culture medium was removed and the cell well was washed thrice with PBS. In the end, 100 μl culture medium containing CCK-8 (10%) was added into each well for 2 h, and the absorbance was measured at 450 nm by using a microplate reader (Thermo, USA).

2.4 Histology

The short-term toxicity of IR-820 doped polymer nanoparticles was evaluated through histological analysis evaluations. 24 h after the intravenous injection of 300 μl nanoparticles (1 mg/mL in 1X PBS, which is also the concentration of nanoparticles we used for the following *in vivo* imaging) and (only)1X PBS (as control), mice with and without treatment (as another control) were sacrificed, and their major organs (heart, liver, kidney and spleen) were removed. Tissues were fixed in 10% formalin, embedded in paraffin, sectioned, and stained with hematoxylin and eosin. The histological sections were imaged under an inverted optical microscope for analysis.

2.5 Macro in vivo imaging studies

All *in vivo* experiments were performed in compliance with Zhejiang University Animal Study Committee's requirements for the care and use of laboratory animals in research. 18-21 g female nude mice were used for macro *in vivo* imaging studies. IR-820 doped polymer nanoparticles in PBS (1X, pH = 7.4) were intradermally injected into the left forepaw of a sedated nude mouse to perform SLN mapping. In addition, nude mice were administered with 300 μl of nanoparticles via tail vein injection and anesthetized with pentobarbital at various time points after the injection for whole-body functional bioimaging. All the NIR imaging was performed under the aforementioned Maestro *in vivo* optical imaging system.

2.6 Microscopic imaging of tissue-equivalent phantom

The synthesis of nanoparticle doped phantom is as following. 0.4 g of gelatin was added to 4 ml of DI water at 60 °C, and 100 μl of IR-820 doped polymer nanoparticles was added into the solution after the gelatin was totally dissolved by vigorous magnetic stirring. It was transferred to a dish, and kept at 4 °C for 2 h. A cylindrical solid-state phantom was then ready for imaging. A control group (without the adding of IR-820 doped polymer nanoparticles) was also prepared, accordingly. The phantoms were then imaged with an upright laser scanning confocal microscope under the 635 nm-CW laser excitation. The average power of excitation light after the water-immersed objective (20X, NA = 1, Olympus) was about 1.3 mW. The confocal aperture (C.A, the size of confocal pinhole) and the scan speed were set to 358 μm and 10 μs/pixel (512 X 512 pixels per frame), respectively.

#222817 - $15.00 USD Received 10 Sep 2014; revised 22 Oct 2014; accepted 23 Oct 2014; published 28 Oct 2014

2.7 Microscopic in vivo imaging studies

8-week-aged female BALB/c mice were then used for microscopic *in vivo* imaging. They were intravenously injected with 300 μl of IR-820 doped polymer nanoparticles via their tail vein. The upright laser scanning confocal microscope (635 nm-laser excited) was adopted for the microscopic imaging of blood vessels in the mouse ear, as well as blood vasculature in the mouse brain. For ear imaging, the average power of the excitation laser after the water-immersed objective (20X, NA = 1, Olympus) was about 1 mW. The C.A was set to 344 μm. The scan speed was set to 2 μs/pixel (512 X 512 pixels per frame). For brain imaging, the nanoparticles treated mice were anesthetized with pentobarbital, and the skulls of the mice were opened up through microsurgery. A metal ring with a handle was mounted onto the mouse brain. A round thin cover glass slide was then embedded in the metal ring and directly adhered to the mouse brain through dental cement. We make sure the brain was flattened by the cover glass slide, which is helpful to improve the microscopic imaging quality. The metal ring was then connected to a metal plate with a handle, via handle-handle fix. Since the metal plate was very heavy, this configuration could keep the mouse's head immobilized during the whole imaging process. Water was smeared between a long work distance (2 mm) water-immersed objective (20X, NA = 1, Olympus) and the top of the cover slide surrounded by the metal ring. The C.A of the confocal microscope was set to 600 μm, and the scan speed was set to 2 μs/pixel (512 X 512 pixels per frame).

3. Results and discussion

3.1 Characterization of IR-820 doped polymer nanoparticles

Figure 2(a) shows a typical TEM picture of IR-820 doped polymer nanoparticles. Since the electron quantities of the atoms constituting polymer nanoparticles and IR-820 molecule, are not very large, the contrast of the image is not high and the contour of the polymer nanoparticles is not very clear [34]. However, we could still discriminate the nanoparticles from the background, and they were indicated by circles in the TEM picture. The nanoparticles have a spherical morphology with an average size of ~45 nm. To verify IR-820 molecules have been encapsulated in the polymer nanoparticles, a drop of ethanol solution of IR-820 and a drop of aqueous solution of IR-820 doped polymer nanoparticles were slowly evaporated on a glass slide. After dried, they were directly imaged with the Maestro *in vivo* optical imaging system as mentioned, and the excitation wavelength was 704 nm. The fluorescence signal was extracted by a long-pass filter, which could also cut off the residual excitation light. A liquid-crystal tunable filter was automatically tuned from 740 nm to 900 nm with 10 nm increments, and the fluorescence intensity and image at each wavelength were recorded by the cooled monochrome CCD camera. As shown in Fig. 2(b), the fluorescence from the aggregates of IR-820 doped polymer nanoparticles could be clearly observed, and it was much brighter than that from the aggregates of IR-820 powder (could hardly be observed), from which we know that the IR-820 molecules have been efficiently encapsulated in the polymer nanoparticles. Otherwise, the fluorescence from the aggregates of the IR-820 doped polymer nanoparticles should be as weak as that from the aggregates of IR-820 powder, which was attributed to a phenomenon called "aggregation caused quench" (ACQ) [35]. Furthermore, the experimental results illustrated hydrophilic polymeric coating could protect hydrophobic IR-820 against denaturalization induced by the environment (e.g. oxidation), making the entire nanoparticles optically stable.

#222817 - $15.00 USD Received 10 Sep 2014; revised 22 Oct 2014; accepted 23 Oct 2014; published 28 Oct 2014

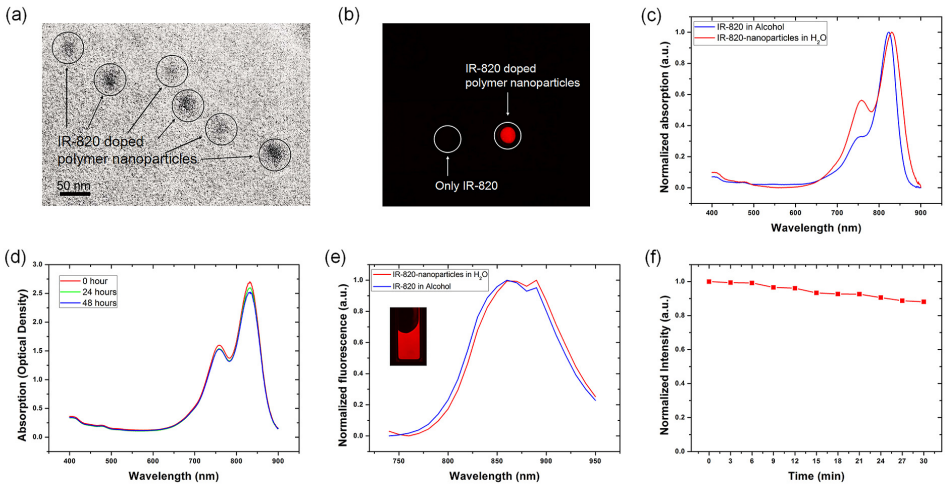

Fig. 2. (a) TEM image of IR-820 doped polymer nanoparticles. (b) Fluorescence imaging picture of the dried powder of (only)-IR820 and IR-820 doped polymer nanoparticles (excitation wavelength: 704 nm). (c) Normalized absorption spectra of IR-820 in ethanol solution and the aqueous solution of IR-820 doped polymer nanoparticles. (d) Absorption spectra of the IR-820 doped polymer nanoparticles in saline solution at various time points (0 h, 24 h and 48 h). (e) Normalized fluorescence spectra of IR-820 in ethanol solution and the aqueous solution of IR-820 doped polymer nanoparticles (excitation wavelength: 704 nm). The inset shows that NIR fluorescence imaging of IR-820 doped polymer nanoparticles in water, under 704 nm excitation. (f) Time trace of fluorescence intensity of IR-820 doped polymer nanoparticles, which was excited by 704 nm-light for half an hour.

The normalized linear absorption spectra of IR-820 in ethanol solution and aqueous solution of IR-820 doped polymer nanoparticles are shown in Fig. 2(c). The absorption peak wavelength (831 nm) of IR-820 doped polymer nanoparticles (in water) has about 7 nm red-shift compared with that (824 nm) of (only)-IR-820 (in ethanol). In addition to optical properties, chemical stability of NIR fluorophores is also very important, which can greatly affect their successful applications in *in vivo* animal studies. In our experiment, UV-vis absorption spectra of IR-820 doped polymer nanoparticles in PBS (1X, pH = 7.4) were monitored to evaluate their stability at different time points (0 h, 24 h, and 48 h). As shown in Fig. 2(d), the absorption spectra of nanoparticles kept very well in saline solution even after 24 h and 48 h, and the optical density of their peak wavelength also did not decrease distinctly, indicating aggregation of the nanoparticles did not occur, and they could keep chemically stable in saline solution for long time. Figure 2(e) shows the fluorescence spectra of IR-820 in ethanol solution and aqueous solution of IR-820 doped polymer nanoparticles, which were measured with the aforementioned Maestro *in vivo* optical imaging system under the 704 nm excitation. Both of the samples show a fluorescence peak wavelength around 860 nm. The fluorescence signal of IR-820 doped polymer nanoparticles mainly located in the "optical transmission window" of biological tissue (700 - 900 nm), which demonstrates that the NIR fluorescent nanoparticles have the deep-tissue imaging potentials. The quantum yield of IR-820 doped polymer nanoparticles was measured by using a methanol solution of indocyanine green dye (fluorescence quantum yield of 0.12 [36]) as a reference, and was found to be 0.05 (not low for NIR nanoparticles). We further did a fluorescence stability test of IR-820 doped polymer nanoparticles under continuous light illumination. As shown in Fig. 2(f), even excited by 704 nm-light (from the aforementioned Maestro *in vivo* optical imaging system) for half an hour, the fluorescence intensity of nanoparticles was still higher than 85% of the original intensity. The photobleaching was negligible after the long time excitation, indicating IR-820 doped

#222817 - $15.00 USD Received 10 Sep 2014; revised 22 Oct 2014; accepted 23 Oct 2014; published 28 Oct 2014

polymer nanoparticles possess stable fluorescence properties, which is very useful for long time dynamic bio-imaging.

3.2 Toxicity of IR-820 doped polymer nanoparticles

Figure 3(a) shows the relative viabilities of HeLa cells treated with IR-820 doped polymer nanoparticles after 24 h. The cells treated with nanoparticles maintained very high viabilities, and it was still larger than 95% even when the concentration of polymer nanoparticles was as high as 4 μg/ml. Furthermore, a histopathology examination shows that there was no inflammation or abnormalities of the major organs (Fig. 3(b)) during the accumulation of IR-820 doped polymer nanoparticles via the blood circulation 24 h post-administration, suggesting that the nanoparticles are very biocompatible. The low cytotoxicity and high biocompatibility of IR-820 doped polymer nanoparticles make them as a good candidate for various *in vivo* bio-imaging applications.

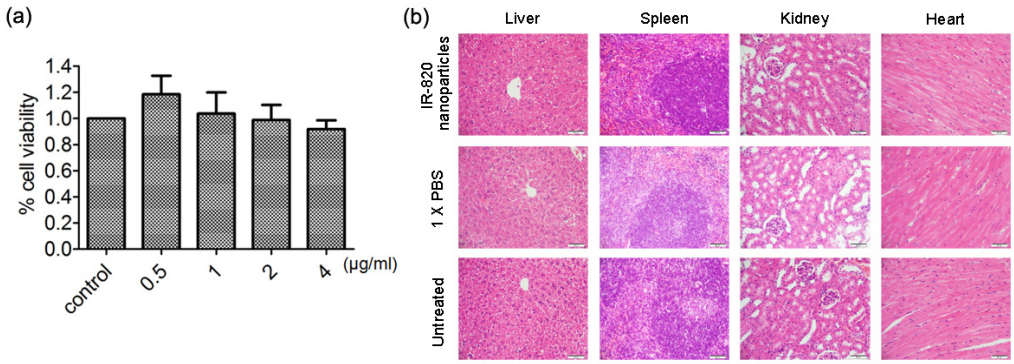

Fig. 3. (a) Viability of HeLa cells after incubation with IR-820 doped polymer nanoparticles for 24 h. (b) Histological examination of liver, kidney, spleen and heart stained with haematoxylin and eosin. Tissues were excised from BALB/c mice 24 h post the treatment with nothing, PBS and IR-820 doped polymer nanoparticles, respectively. Scale bar: 50 μm.

3.3 IR-820 doped polymer nanoparticles for SLN mapping of nude mice

Accurate identification and biopsy of SLN are very significant in medicine. Some nanoparticles [37–39] (e.g. QDs and gold nanoparticles) have already been used for SLN mapping, and we present another approach in this work. 50 μl of IR-820 doped polymer nanoparticles in PBS (1X, pH = 7.4) was injected intradermally into the left forepaw of nude mice, and the mice were imaged with the *in vivo* optical imaging system under the 704 nm excitation. The NIR fluorescence signals from IR-820 doped polymer nanoparticles were colored in red and the background autofluorescence from mice body was colored in green (as shown in Fig. 4(a)-4(f)). An image of a typical mouse before injection (as a reference) was shown in the inset of Fig. 4(h), and only autofluorescence could be observed. Some NIR fluorescence signals appeared in the SLN site of the mouse 5 mins post sample treatment (Fig. 4(a)), due to the rapid diffusion of nanoparticles from the injection to lymphatics. As the time went by, the intensity of signals became stronger in the SLN site (Fig. 4(b) and 4(c)), and the maximum of the signals intensity appeared after 60 mins (Fig. 4(c)). After that, NIR fluorescence signals decreased gradually (Fig. 4(d)-4(f)), because nanoparticles migrated from the SLN after 60 mins. Figure 4(h) shows the changes of NIR signal intensity of nanoparticles in the SLN site, which was consistent with our previously reported measure of this process by using other nanoparticles [32,34]. Furthermore, the fluorescence spectrum obtained from the SLN site (Fig. 4(g)) verified that the NIR fluorescence signals were indeed emitted from IR-820 doped polymer nanoparticles. The results demonstrated that IR-820 doped polymer nanoparticles can be used as NIR optical probes for SLN mapping of live animals.

#222817 - $15.00 USD Received 10 Sep 2014; revised 22 Oct 2014; accepted 23 Oct 2014; published 28 Oct 2014

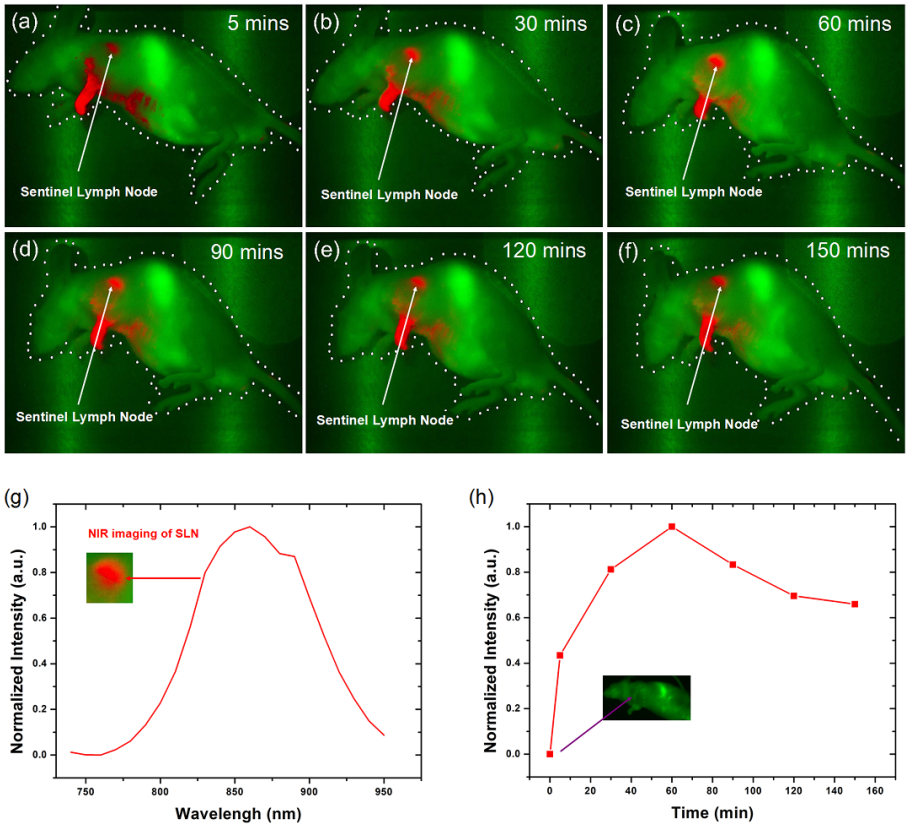

Fig. 4. NIR fluorescence imaging of a nude mouse with IR-820 doped polymer nanoparticles intradermally injected into the left forepaw pad at various time points post-injection. (a)-(f) NIR fluorescence imaging (exposure time: 5000 ms) of the mouse: 5, 30, 60, 90, 120, and 150 mins after the injection of nanoparticles. (g) NIR fluorescence spectrum from SLN, (Inset) Magnified NIR imaging of SLN. (h) The normalized NIR signal intensity of nanoparticles in the SLN site of the mouse: before the injection, 5, 30, 60, 90, 120, and 150 mins after the injection of nanoparticles. The inset shows the NIR fluorescence imaging (exposure time: 5000 ms) of the mouse before the injection.

3.4 IR-820 doped polymer nanoparticles for whole-body functional bioimaging

To verify the capacity of IR-820 doped polymer nanoparticles in NIR whole-body *in vivo* imaging, 0.3 ml of nanoparticles in PBS (1X, pH = 7.4) was intravenously injected into a nude mouse. Another nude mouse without any treatment was used as a control. The two mice were then anesthetized with pentobarbital at various time points after the injection, and the sedated animals were imaged using the aforementioned Maestro *in vivo* optical imaging system. Figure 5(a)-5(f) show the NIR fluorescence imaging of the treated mouse (the right one) and the untreated mouse (the left one) at various time points of post-injection. Based on the imaging results and data treatment, the NIR fluorescence signals (with peak wavelength at 860 nm) from IR-820 doped polymer nanoparticles were colored in red and the background autofluorescence (e.g. from skin) was colored in green. Their normalized spectra could be distinguished from each other very easily (shown in Fig. 5(g)), which indicated the NIR *in vivo* imaging has very high contrast. One hour after the sample treatment, intense NIR fluorescence signals appeared in the liver of the treated mouse, and nanoparticles have already accumulated in the liver through blood circulation. As time went by, the intensity of the signals in the liver decreased gradually, indicating the mouse was metabolizing the nanoparticles all the time. Interestingly,

#222817 - $15.00 USD Received 10 Sep 2014; revised 22 Oct 2014; accepted 23 Oct 2014; published 28 Oct 2014

23 h post the sample treatment, NIR signals could be observed in the intestinal tract of the treated mouse, illustrating nanoparticles were excreted from the mouse body through its hepatobiliary transport. 120 h post the sample treatment, no NIR signals could be observed from the treated mouse, and most nanoparticles have been cleared from the mouse body. The background fluorescence of the reference mouse and nanoparticles treated mouse was different. One possible reason is that the intensity distribution of excitation light on the two mice was slightly different. Since the CCD detector in the Maestro *in vivo* optical imaging system was very sensitive, the slight difference was magnified, which made the background fluorescence of the two mice seem different. It is worth noting that both liver and intestinal tract were deep in the mouse body, and NIR fluorescent nanoparticles demonstrated their capacity in deep-tissue optical bioimaging. 80 days after the injection of the nanoparticles, no apparent pathological differences in shape, weight, eating, drinking, exploratory behavior or activity were observed between the two mice (with and without sample treatment). The results indicated the IR-820 doped polymer nanoparticles have very little toxicity, which may facilitate their clinical applications in disease diagnosis and therapy.

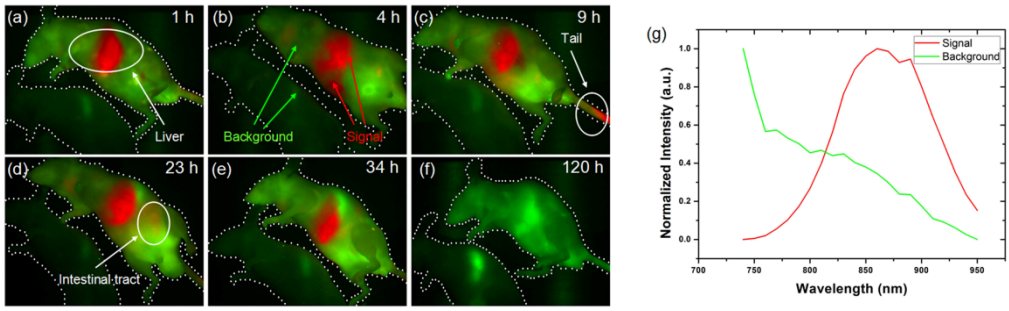

Fig. 5. (a)-(f) NIR fluorescence imaging of a nude mouse intravenously injected with IR-820 doped polymer nanoparticles at various time points of post-injection (exposure time: 5000 ms). (g) NIR fluorescence spectra of the signal and background from mice.

3.5 Study of deep microscopic imaging capacity of IR-820 doped polymer nanoparticles in phantom

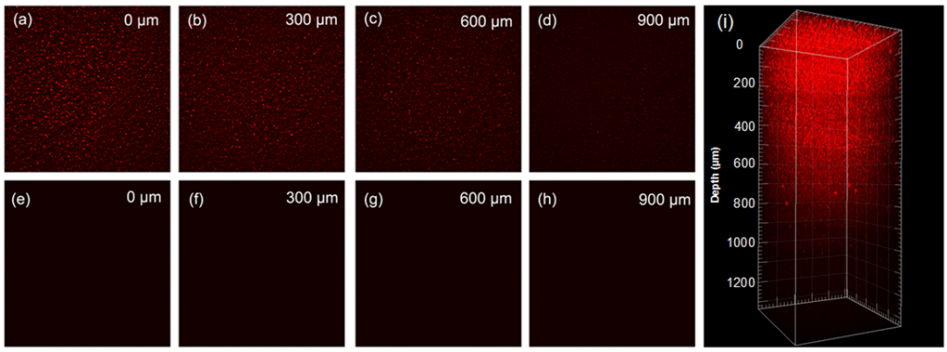

Fig. 6. Fluorescence microscopic images of tissue-equivalent phantom mixed with (a-d) and without (e-h) IR-820 doped polymer nanoparticles at some vertical depths: 0 μm, 300 μm, 600 μm, 900 μm. (i) A 3D reconstructive image showing the distribution of IR-820 doped polymer nanoparticles in the tissue-equivalent phantom.

Laser assisted microscopy provides higher spatial resolution than macro imaging, but its imaging depth is not comparable with that of macro imaging. Tissue-equivalent phantom experiments were preformed to verify that IR-820 doped polymer nanoparticles have the capacity of deep-tissue microscopic imaging. Figure 6(a)-6(d) show the fluorescence images at different depths of the nanoparticle-doped-phantom, and their reconstructed 3D image is shown

#222817 - $15.00 USD Received 10 Sep 2014; revised 22 Oct 2014; accepted 23 Oct 2014; published 28 Oct 2014

in Fig. 6(i), from which we know that the maximal microscopic imaging depth of NIR fluorescent nanoparticles in phantom is ~1100 μm. As for the control phantom, no fluorescence signals could be observed at any depth of the phantom, under the excitation of 635 nm-CW laser (shown in Fig. 6(e)-6(h)). The experimental results demonstrated that IR-820 doped polymer nanoparticles could be further used for microscopic imaging of thick tissues, as well as small animals.

3.6 IR-820 doped polymer nanoparticles for in vivo microscopic imaging of blood vessels in a mouse ear

IR-820 doped polymer nanoparticles were then utilized as NIR optical nanoprobes for *in vivo* microscopic imaging. Figure 7(a)-7(g) show the fluorescence images of blood vessels in the ear of the mouse at various vertical depths. Due to bright NIR fluorescence of IR-820, as well as low background autofluorescence of tissue under red light-excitation, the signal to noise ratio of all the images was very high, and the structure of blood vessels at any depth of the mouse ear could be observed very clearly. Figure 7(h) shows the corresponding reconstructed 3D image (taken with 2 μm depth increments) of the NIR fluorescent nanoparticles in the blood vessels, from which the vascular architecture in the mouse ear was vividly revealed.

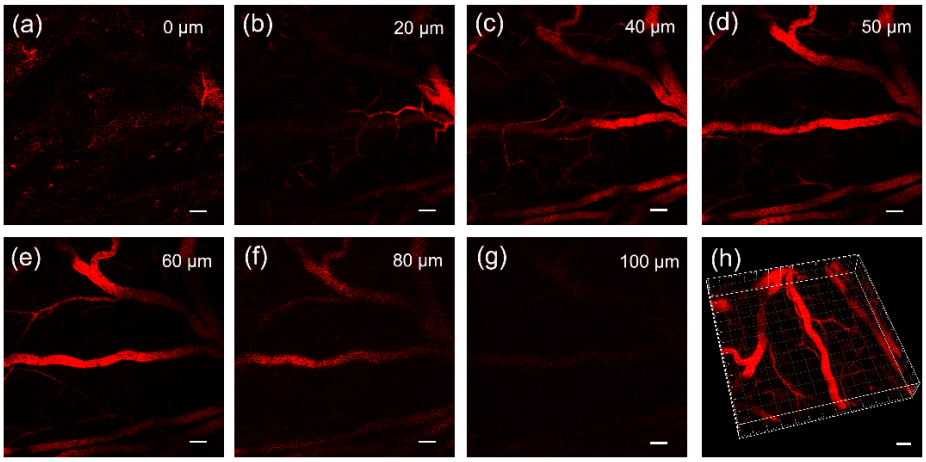

Fig. 7. Fluorescence microscopic images of blood vessels in the mouse ear at various vertical depths (a): 0 μm, (b): 20 μm, (c): 40 μm, (d): 50 μm, (e): 60 μm, (f): 80 μm, (g): 100 μm, and a 3D reconstructive image (h) showing the distribution of the IR-820 doped polymer nanoparticles in the blood vessels in the mouse ear. (Scale bar: 50 μm).

3.7 IR-820 doped polymer nanoparticles for in vivo microscopic imaging of blood vasculature in a mouse brain

We further performed *in vivo* brain imaging of 8 week-female BALB/c mice by using IR-820 doped polymer nanoparticles. Figure 8(a)-8(l) show the fluorescence images of blood vasculature in the brain of the mouse at various vertical depths (below the skull). At the surface of the brain, the average power of the 635 nm-laser after the objective is ~0.8 mW, which is high enough to excite the NIR fluorescent nanoparticles in the blood vasculature. The brightest NIR signal occurred at the vertical depth of 130 μm. With the increasing depth in the mouse brain, the fluorescence signal intensity of IR-820 doped polymer nanoparticles decreased due to scattering and water absorption of the tissue (shown in Fig. 8(d)-8(l)). However, at the depth of 500 μm, the tiny structure of capillary vessels could still be discriminated by virtue of NIR fluorescence from the nanoparticles inside, and the average power of the 635 nm-laser after the objective is ~1.5 mW, which was very safe to the biosamples. Figure 8(m) and 8(n) show reconstructed 3D images (taken with 2 μm depth increments) of IR-820 doped polymer

#222817 - $15.00 USD Received 10 Sep 2014; revised 22 Oct 2014; accepted 23 Oct 2014; published 28 Oct 2014

nanoparticles in the blood vasculature, from which we know that the maximal imaging depth could reach ~500 μm. In a traditional (one-photon) confocal microscopy with UV/blue/green excitation, the imaging depth is very difficult to be deeper than 100 μm. As aforementioned, with the help of less absorption/scattering of red light excitation and NIR emission light in the tissue, deeper imaging capability is achieved in our work, by directly utilizing one-photon confocal microscopy. By improving excitation and detection modes (e.g., making excitation wavelength get closer to the absorption peak of NIR fluorophore, and adopting NIR sensitive PMT to replace NIR insensitive PMT in the confocal microscope), as well as optical feature of fluorophores (e.g., increasing quantum efficiency), imaging depth of this one-photon confocal microscopy can be further increased, which will be very useful to some neurophotonics research and applications.

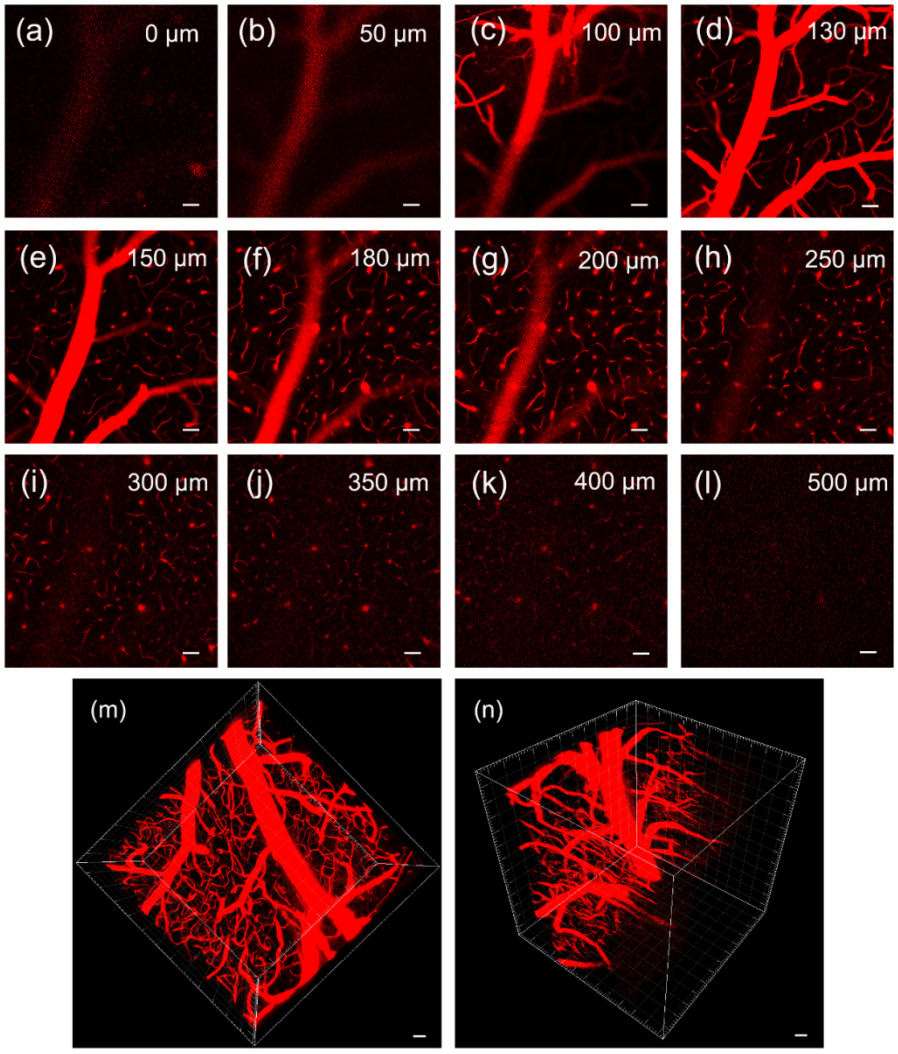

Fig. 8. Fluorescence microscopic images of blood vessels in the mouse brain at various vertical depths (a): 0 μm, (b): 50 μm, (c): 100 μm, (d): 130 μm, (e): 150 μm, (f): 180 μm, (g): 200 μm, (h): 250 μm, (i): 300 μm, (j): 350 μm, (k): 400 μm (l): 500 μm) and 3D reconstructive images (m, n) showing the distribution of the IR-820 doped polymer nanoparticles in the blood vasculature in the mouse brain. (Scale bar: 50 μm).

#222817 - $15.00 USD Received 10 Sep 2014; revised 22 Oct 2014; accepted 23 Oct 2014; published 28 Oct 2014

4. Conclusions

Optically and chemically stable polymer nanoparticles with NIR fluorophores doped were synthesized and utilized as efficient optical nanoprobes for macro/microscopic *in vivo* bioimaging. NIR fluorescent nanoparticles with very little toxicity can be used for SLN mapping and whole-body functional *in vivo* bioimaging. Furthermore, the NIR fluorescent nanoparticles were used for *in vivo* microscopic bioimaging via a confocal microscope with red excitation. The blood vessel architecture in the ear and the brain of mice, which were intravenously injected with nanoparticles, was revealed vividly. The imaging depth of our NIR nanoparticle-assisted one-photon microscopy can reach as deep as 500 μm. NIR fluorescent nanoparticles have great potentials in life sciences and medicine, such as early diagnosis/therapy of tumor.

Acknowledgments

This work was supported by National Basic Research Program of China (973 Program; 2013CB834704 and 2011CB503700), the National Natural Science Foundation of China (61275190 and 91233208), the Program of Zhejiang Leading Team of Science and Technology Innovation (2010R50007) and the Fundamental Research Funds for the Central Universities.

#222817 - $15.00 USD Received 10 Sep 2014; revised 22 Oct 2014; accepted 23 Oct 2014; published 28 Oct 2014